

## Article

# The Relationship between Madden–Julian Oscillation Moist Convective Circulations and Tropical Cyclone Genesis

Patrick Haertel

Department of Earth and Planetary Sciences, Yale University, New Haven, CT 06511, USA;  
patrick.haertel@yale.edu

**Abstract:** The Madden–Julian Oscillation (MJO) is a planetary-scale weather system that creates a 30–60 day oscillation in zonal winds and precipitation in the tropics. Its envelope of enhanced rainfall forms over the Indian Ocean and moves slowly eastward before dissipating near the Date Line. The MJO modulates tropical cyclone (TC) genesis, intensity, and landfall in the Indian, Pacific, and Atlantic Oceans. This study examines the mechanisms by which the MJO alters TC genesis. In particular, MJO circulations are partitioned into Kelvin and Rossby waves for each of the developing, mature, and dissipating stages of the convective envelope, and locations of TC genesis are related to these circulations. Throughout the MJO’s convective life cycle, TC genesis is inhibited to the east of the convective envelope, and enhanced just west of the convective envelope. The inhibition of TC genesis to the east of the MJO is largely due to vertical motion associated with the Kelvin wave circulation, as is the enhancement of TC genesis just west of the MJO during the developing stage. During the mature and dissipating stages, the MJO’s Rossby gyres intensify, creating regions of low-level vorticity, favoring TC genesis to its west. Over the 36-year period considered here, the MJO modulation of TC genesis increases due to the intensification of the MJO’s Kelvin wave circulation.

**Keywords:** Madden–Julian oscillation; tropical cyclone genesis; Kelvin wave; Rossby wave



**Citation:** Haertel, P. The Relationship between Madden–Julian Oscillation Moist Convective Circulations and Tropical Cyclone Genesis. *Climate* **2023**, *11*, 134. <https://doi.org/10.3390/cli11070134>

Academic Editors: Sen Chiao, Das Debanjana, Shaowu Bao and Karle Nakul

Received: 12 May 2023

Revised: 18 June 2023

Accepted: 21 June 2023

Published: 25 June 2023



**Copyright:** © 2023 by the author. Licensee MDPI, Basel, Switzerland. This article is an open access article distributed under the terms and conditions of the Creative Commons Attribution (CC BY) license (<https://creativecommons.org/licenses/by/4.0/>).

## 1. Introduction

### 1.1. Madden Julian Oscillation (MJO) Overview

The MJO is a planetary-scale weather system that generates a 30–60 oscillation in zonal winds and precipitation over the warm waters of the equatorial Indian and Western Pacific Oceans [1–4]. In a typical MJO, a region of enhanced precipitation forms in the Indian Ocean and then moves slowly eastward before dissipating near the Date Line, leaving a largely dry circulation that propagates more rapidly through the Western Hemisphere [5–7]. The MJO has impacts on weather and climate all over the world, including tropical cyclones (reviewed below), monsoons [8–10], atmospheric rivers [11], and the El Niño/Southern Oscillation [12–14]. Because the MJO is considered predictable for several weeks or more, and it has many weather and climate impacts, accurately predicting the MJO and its impacts could lead to improved mid-range weather forecasts [15,16].

### 1.2. MJO Impacts on Tropical Cyclones (TCs)

Numerous studies have shown that the MJO modulates TC genesis, intensification, and/or landfall throughout the tropics. However, the proposed mechanisms differ by study and basin. Here, we review a subset of these studies to sample the diversity of ideas in the scientific literature on this topic.

We start by considering the general vicinity of the Indo-Pacific warm pool, where the MJO is convectively active. Liebmann et al. [17], in one of the earliest studies to consider TC modulation by the MJO, examined populations of tropical depressions, storms, and typhoons in the Western Pacific and Indian Oceans for different MJO phases during 1979–1989. They found that at both 12 N and 12 S, roughly 2–3 times as many systems

occurred during the active phase of the MJO than during the suppressed phase. They found no clear variations in the relative populations of disturbance types, and they concluded that there were more tropical storms and typhoons during the active phase of the MJO because there were more depressions at that time. Kim et al. [18] also examined the impact of the MJO on TCs in the western North Pacific from June to September in 1979–2004. During this time, the MJO convective signal propagated both eastward and northward from the central Indian Ocean. They found that there were significantly more TCs when the MJO enhanced convection, and there were also more landfalling TCs in Korea and Japan during the MJO active phases. Chen et al. [19] helped to explain the mechanism of MJO modulation of TCs by examining precursory tropical disturbances (PTDs) in the western North Pacific (WNP) for 1990–2014 using the ERA-Interim reanalysis. They calculated the ratio that developed into TCs and typhoons for different phases of the MJO, the El Niño/Southern Oscillation (ENSO), and equatorial Rossby waves (ERWs). They used a regional MJO index for the WNP based on space- and time-filtered OLR for 0–15 N and 110–170 E. They found that significantly more PTDs developed into tropical storms during the MJO active phase than inactive (0.42 vs. 0.32, respectively), with relative vorticity perturbations at 850 hPa and relative humidity anomalies at 700 hPa as primary and secondary factors for developing TCs.

The modulation of TCs by the MJO in the Indian Ocean is especially strong. Hall et al. [20] examined TC genesis to the northwest and northeast of Australia and noted that three to four times as many TCs formed during the active phase of the MJO than during the suppressed phase. They also noted that the MJO enhanced both low-level vorticity and precipitation during the times when TC genesis was favored. Bessafi and Wheeler [21] also examined TC genesis in the southern Indian Ocean, but to the west of 100 E. They also found TC genesis was enhanced during the active phase of the MJO by a factor of 2.6 over the inactive phase, and that TCs preferentially occurred in regions with low-level vorticity in the Rossby wave component of the MJO circulation. Krishnamohan et al. [22] studied the impact of the MJO on TC genesis in the North Indian Ocean between 60 and 100 E from 1979 to 2008. They found that when the MJO was active, 81% of TCs formed in the convective phase (i.e., when the real-time multivariate MJO (RMM) index [23] was in phases 1–4). TC formations clustered around cyclonic vorticity anomalies, mostly in regions with low vertical wind shear. Girishkumar et al. [24] also examined MJO impacts on TC formation in the North Indian Ocean, focusing on the Bay of Bengal region for 1985–2012. They found that 2.5 more TCs formed in MJO phases 3–5 than in 1–2 and 6–8 combined, and that 71% of TCs undergoing rapid intensification occurred in MJO phases 3–5. They also noted that higher relative humidity enhanced low-level vorticity, and lower wind shear enhanced TC formation and rapid intensification. Bhardwaj et al. [25] examined the impacts of the MJO on TCs over the Bay of Bengal (BoB) from 1974 to 2015. They noted a bimodal annual TC distribution with maxima in April–June (AMJ) and October–December (OND). In AMJ, there was enhanced convection over the BoB in MJO phases 2–4 as well as more TCs. In OND, TCs were enhanced in the southwest BoB in phases 2–3 and the northeast BoB in phases 4–5. A combination of enhanced convection and higher mid-level relative humidity increased low-level cyclonic vorticity, and reduced vertical wind shear contributed to the enhancement of TCs during the active periods of the MJO.

The MJO is also known to modulate TCs in the Eastern Pacific and Atlantic basins, but in a different manner, as these regions are far from the MJO's convectively active region. Maloney and Hartmann [26] considered how the MJO modulates TC genesis in the Eastern Pacific using an MJO index based on an 850 hPa equatorial zonal wind. They found that more TCs formed when there were near equatorial westerly wind perturbations and off-equatorial enhanced convection in phase 2 of the MJO. They noted that the equatorial wind perturbations associated with TC genesis perturbations propagated in from the MJO's convectively active region (Indian Ocean and West Pacific) through Kelvin wave dynamics. They concluded that the MJO enhanced TC genesis in the East Pacific by increasing low-level vorticity and reducing vertical wind shear. These effects were so strong that more than

four times as many hurricanes formed during the westerly phase of the MJO than during the easterly phase. Barrett and Leslie [27] considered the impact of the MJO on TC genesis in the Eastern Pacific and North Atlantic. They used an MJO index based on a 200 hPa velocity potential, because it has a signal that circumnavigates the globe, which is likely associated with a propagating Kelvin wave in the western hemisphere. They found that TC genesis is enhanced with negative velocity potential (i.e., enhanced 200 hPa divergence), and that the MJO caused significant changes to TC genesis, hurricane genesis, and landfall. Klotzbach and Oliver [28] considered variations in North Atlantic TCs by the MJO phase for the period 1905–2011. They used a surface pressure-based MJO index, constructed to mimic the RMM index for 1979–2011. They found that throughout the last century, there was a significant increase in accumulated cyclone energy and major hurricanes during phases 1–3 of the MJO than in phases 5–7. Reduced zonal vertical shear, upward motion, and positive 700 hPa relative humidity anomalies accompanied the increases in TC activity.

Several studies have attempted to explain the MJO modulation of TCs in terms of the empirical genesis potential index (GPI). Camargo et al. [29] attempted to explain variations in TC genesis associated with the MJO in terms of the Emanuel–Nolan GPI. They found that genesis potential anomalies track the MJO precipitation signal, and are maximized on the poleward edge, similar to patterns in TC genesis anomalies. They concluded that roughly half of the modulation of TCs is explained by variations in the GPI, and suggested variations in the occurrence of precursor disturbances could also be important on intraseasonal time scales. The GPI allowed for partitioning into different terms; it revealed that mid-level humidity variation was the most important factor, followed by low-level relative vorticity anomalies, for the purpose of explaining TC genesis anomalies. Wang and Moon [30] related TC genesis to the MJO phase for November through April of 1979–2014 in the Indian Ocean and West Pacific. They used an MJO index based on outgoing longwave radiation (OLR) between 0 and 20 S. They noted that TC genesis anomalies existed on the poleward edges of the MJO precipitation anomaly, and extended westward. They developed an intraseasonal GPI, with the most important factors being the Coriolis parameter multiplied by the relative vorticity at 850 hPa, 500 hPa pressure velocity, and the zonal wind shear between 850 and 200 hPa. This intraseasonal GPI explained the vast majority of TC variability in the southern hemisphere in the Indian and West Pacific Oceans. They concluded that most of the change in TC genesis resulted from low-level vorticity associated with the MJOs Rossby gyres.

In summary, the MJO has been found to modulate TCs in every basin, with most studies reporting amplifications in the frequency of occurrence of 2–4 during the active phase relative to the suppressed phase of the MJO. Various mechanisms have been suggested, including the generation of more precursor disturbances, enhanced low- and mid-level vorticity and/or relative humidity, reduced vertical wind shear, upward motion, upper-level divergence, and a higher probability of precursor disturbances growing into tropical storms and hurricanes. In the Indian Ocean and West Pacific, many of these impacts have been associated with the MJO's low-level Rossby gyres, and in the East Pacific and Atlantic, changes have been attributed to Kelvin wave dynamics.

### 1.3. Motivation

Most studies that have examined MJO impacts on TCs have focused on one particular region and considered MJO-related changes to several atmospheric variables. Because different studies have examined different regions and variables, and few studies have sought to understand the dynamics underlying MJO-induced changes to atmospheric variables, a complete dynamical analysis of the MJO's impacts on TCs has yet to be presented. This study aims to lay the groundwork for such an analysis, by viewing the MJO changes to TC genesis in the frame of reference of the MJO's convective envelope, and relative to the two dynamical components of the MJO's circulation: the Kelvin wave and the Rossby wave. We follow the method of Haertel [31] by partitioning the MJO's circulation in Rossby and Kelvin waves for each developing, mature, and dissipating stage of the convective envelope. We then consider the impacts of each component of the circulation on TC formation for

each stage. Note that while there are many types of synoptic-scale waves embedded with the MJO's convective envelope, including Kelvin waves, westward inertio-gravity waves, mixed Rossby gravity waves, and Rossby waves [32–34], the focus of this paper is not on these waves. Rather, this paper discusses the planetary-scale convectively generated MJO circulation, which projects strongly onto only Kelvin and Rossby waves, with only weak contributions from other equatorial wave types.

This paper is organized as follows. Section 2 describes the data and the methods of analysis. Section 3 provides an analysis of how the Kelvin and Rossby wave components of the MJO's circulation alter TC genesis, and of how the TC patterning of the MJO has changed in recent decades. Section 4 summarizes the results and relates them to those of other studies of the MJO impacts on TCs.

## 2. Materials and Methods

### 2.1. Data

Three data forms are used in this study: satellite observations of precipitation, atmospheric-sounding data, and tracks of TCs. The data are analyzed for the period 1979–2014, which is the time of overlap of all three of the datasets in which there is good spatial and temporal coverage.

#### 2.1.1. GPCP Rainfall Estimates

In order to identify MJO precipitation envelopes, we make use of the Global Precipitation Climatology Project (GPCP) pentad product, version 2 [35,36], which has good data coverage for 1979–2014. These data provide satellite-based estimates of rain rates over 73 5-day intervals per year. We previously used the daily GPCP data, which were available for a shorter time period, to identify the MJO envelopes [7]; however, owing to the long period of the MJO, we found that a 5-day resolution is sufficient to resolve its convective life cycle.

#### 2.1.2. IGRA Sounding Data

Atmospheric-sounding data were taken from the Integrated Global Radiosonde Archive Version 2 (IGRA [37,38]). Stations were included from 35 S to 35 N. The zonal and meridional wind components and temperature were interpolated to a 25 hPa resolution, averaged into pentads to match the time resolution of GPCP data, and then high-pass-filtered for periods shorter than 75 days. Filtered data were analyzed in MJO-relative coordinates for each developing, mature, and dissipating stage of the convective envelope, following Haertel et al. [7]. IGRA version 2 data were kindly provided by Maria Gehne of the NOAA Physical Sciences Laboratory.

There are several reasons why raw-sounding data were used instead of a model reanalysis. First, the author wished to create a purely observational composite of the MJO circulations. Reanalysis products are a somewhat mysterious combination of observations and model forecasts; in data-sparse regions, such as where the MJO occurs, they are particularly likely to weigh the model forecast heavily. Models have a long history of having problems in simulating the MJO [39]; obtaining realistic vertical structures and Kelvin wave components are particularly challenging [40]. While it is true that the sounding data are more horizontally sparse than reanalysis, owing to our method of compositing in an MJO frame of reference, sounding stations are put in different locations for different MJOs and different days in a given stage, thereby increasing spatial coverage. Moreover, in this paper, we are interested in the planetary-scale MJO circulation, and the sounding data are more than adequate for resolving that circulation.

#### 2.1.3. IBTRACS Tropical Cyclone Data

In order to determine how the MJO modulates TC genesis, we make use of the International Best Track Archive for Climate Stewardship (IBTRACS) data [41,42], which combines recent and older TC data from many agencies. We define an instance of TC

genesis as when the surface wind speed for a particular storm first reaches 35 knots. As with sounding and satellite observations, TC genesis data are analyzed within the frame of reference of the MJO precipitation envelope.

## 2.2. Identifying and Compositing MJOs

We identify MJOs following the method of Haertel [43], who used a slightly modified version of the approach developed by Haertel et al. [7]. First, GPCP rainfall data for the period 1979–2014 are bandpass-filtered for periods of 15–75 days. Then, contiguous regions of filtered equatorial rainfall perturbations exceeding 0.7 mm/day in amplitude that propagate eastward at least 90 degrees in longitude during their lifetime are objectively identified and tracked. This method identifies 154 MJO precipitation envelopes during the 36-year period or an average of 4.27 MJOs per year. The MJO precipitation envelopes generally form in the Indian Ocean and dissipate in the Western Pacific, but the precise locations vary from one MJO to the next, putting individual sounding stations in different locations for different MJOs in the MJO relative coordinate system. Figure 1 shows a composite time-longitude series of rainfall for all the cases considered. A precipitation envelope propagates slowly eastward by more than one-third of the way around the world. A linear approximation of the path is shown, with the first third defining the developing stage of the precipitation envelope, the second third defining the mature stage, and the last third defining the dissipating stage. Below, we show average circulations for each stage of the MJO precipitation envelope as revealed by sounding observations. Note that this MJO composite is unconventional in the sense that no model forecast is used in its construction, which makes it useful for evaluating model representations of the MJO without bias.

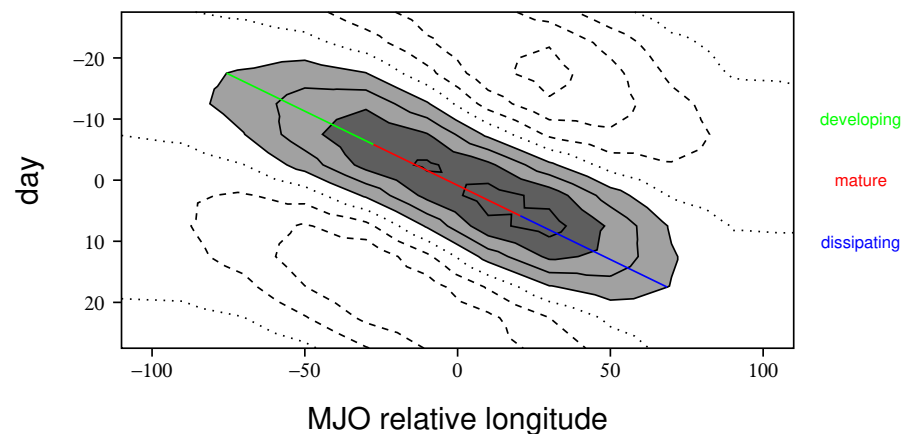


**Figure 1.** Time-longitude series of rainfall for the composite MJO. The contour interval is 0.4 mm/day and values greater than 0.4 (1.2) mm/day are shaded light (dark) gray. The path of the center of the convective envelope is shown with a color-coded line for each stage.

## 2.3. Kelvin/Rossby Wave Decomposition

The focus of this paper is on relating the impacts of the MJO on TCs to convectively generated MJO circulations. To illustrate our method of decomposing MJO circulations into fundamental dynamical components, we apply it in a simple linear simulation. Consider an equatorial heat source, with a meridional Gaussian radius of 10 degrees latitude, and a zonal Gaussian radius of 30 degrees longitude. We suppose that this heat source is stationary, has a duration of 5 days, and occurs in a convective basic state, in which convective heating cancels 70% of the adiabatic temperature change due to vertical motion, which is one way of interpreting the reduced equivalent depth of moist tropical atmospheric disturbances [33,34,44,45]. We simulate the atmospheric response to this heating using the linear tropical model of [46], which has a rigid upper boundary at 150 hPa and a heating profile that excites only the first baroclinic mode so that solutions can be interpreted in terms of shallow water dynamics [47]. In Figure 2, we plot average tropospheric temperatures

(contours) and the difference between the 850 hPa and 200 hPa flow (vectors), because these variables illustrate the first baroclinic mode circulations nicely, and they can easily be compared with observed circulations for the MJO (see below).

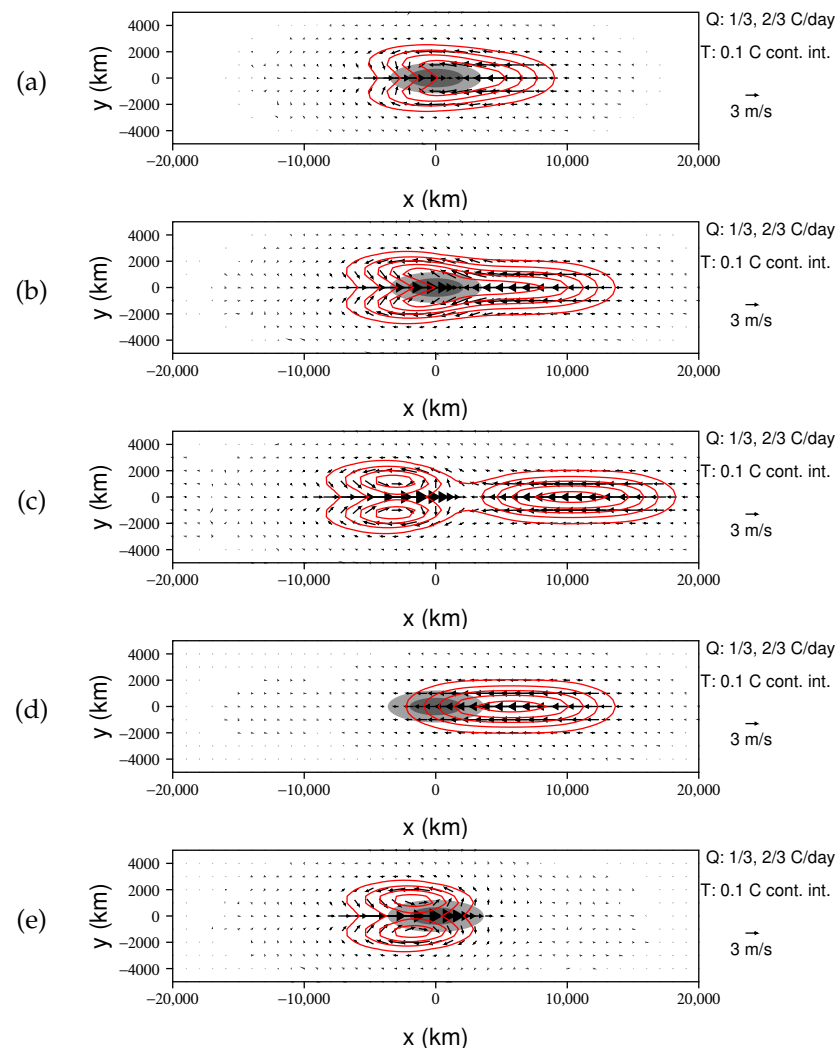


**Figure 2.** A simulation of the linear atmospheric response to MJO-like heating. Average tropospheric temperature is contoured with a 0.1 C contour interval, regions of heating greater than 0.333 (0.667) C/day are shaded light (dark) gray, and vectors indicate the difference between 850 hPa and 200 hPa flow. Panels (a–c) are for 3, 5, and 7 days, respectively. Panel (d) shows the Kelvin wave projection for day 5, and Panel (e) shows the Rossby wave component for day 5.

After 3 days, the heating (gray shaded region) warmed the troposphere in its vicinity and generated low-level zonal wind convergence (Figure 2a). Wind vectors to the east of the heating were parallel, but those to the west exhibited meridional convergence owing to the beta effect. After 5 days, the warm anomaly spread more rapidly to the east, and winds maintained a similar pattern (Figure 2b). Two days after the heating shut off (day 7), the dynamical nature of the circulations became evident, i.e., a Kelvin wave propagated eastward, and Rossby gyres propagated westward (Figure 2c). These waves were superposed on day 5, and in order to isolate their structures at this time, we applied the Kelvin wave projection of Haertel [31], yielding the field shown in Figure 2d. Note that the Kelvin wave had the same structure on day 5 (Figure 2d) as it did on day 7 (Figure 2c), it just moved eastward with time. By subtracting the Kelvin wave component (Figure 2d) from the total field (Figure 2b), we obtained the Rossby wave solution for day 5 (Figure 2e), which also had the same structure as on day 7, but this wave moved westward with time.

Thus, we see that the filter effectively isolates the two fundamental dynamical components of the atmospheric response to the heating, even when they are superposed. Below we apply this filter in the same manner to isolate Kelvin and Rossby wave components of the MJO's circulation; it is even more necessary in that case because both positive and negative heating perturbations are present in the MJO, and the waves they excite propagate around the world, leaving a more complicated superposition of waves than in the simple simulation shown in Figure 2.

One other point about the simulation is worthy of mention. In order to interpret MJO circulations, many previous studies have used the Matsuno–Gill (MG) model [48,49], which resembles the solution shown in Figure 2b. This solution also has a Kelvin wave component that extends eastward from the heat source and a Rossby wave component that extends westward, but it differs in several important ways from the simple simulation. The MG solution is for a steady state, and the zonal extent of the Rossby and Kelvin wave components depends on the damping coefficient (i.e., the waves decay as they propagate eastward and westward). In contrast, our simulation has propagating Kelvin and Rossby wave fronts and there is no damping. As is noted below, similar fronts are present in the MJO, which calls into question the applicability of the MG model to the MJO.

### 3. Results

#### 3.1. Composite MJO Circulations

Before we discuss how the MJO impacts TC genesis, we discuss the circulations in the composite MJO and their dynamical decomposition. Our compositing method is unique in that it presents circulations in a coordinate system centered on the convective envelope, it uses no model forecast to supplement observations, and it has phases based on the convective life cycle. Haertel et al. [7] previously constructed a similar composite MJO, and Haertel [31] presented a dynamical decomposition of its circulations, but those results were based on only 12 years of data with fewer sounding stations than are included here. The improvements to the data presented in this paper reduce the noise in the composite MJO structure, making the individual dynamical components more clear.

During the developing stage, the equatorial troposphere is cool to the west of the MJO, with westerly low-level flow (Figure 3a). The Kelvin wave projection (Figure 3b) reveals that this is a negative phase Kelvin wave that was generated by suppressed convection to the east of the MJO, which has propagated around the world (see also the linear simulations in [31]). A smaller and weaker positive phase Kelvin wave is also beginning to grow out of the developing convective envelope, which manifests itself as a positive temperature anomaly with the easterly low-level flow on the eastern edge of the precipitation region (Figure 3a,b). The strongest feature in the Rossby wave circulation (Figure 3c) is a pair of negative-phase Rossby gyres with the anticyclonic flow on the poleward edges of the suppressed region to the east of the MJO (Figure 3c). These also may be interpreted as a response to the suppressed convection to the east of the MJO. By and large, the negative phase features are what linear dynamics would predict as responses to the suppressed convection ahead of the MJO, which has been occurring for some time by the developing stage and is now dissipating (look 100 degrees to the east of the green line in Figure 1). These features are also reminiscent of the features in our linear simulation on day 7 but of opposite signs (Figure 2c). Finally, we note that weak positive Rossby gyres are starting to grow on the western edge of the growing convective envelope, consistent with the predictions of linear dynamics (Figure 3c).

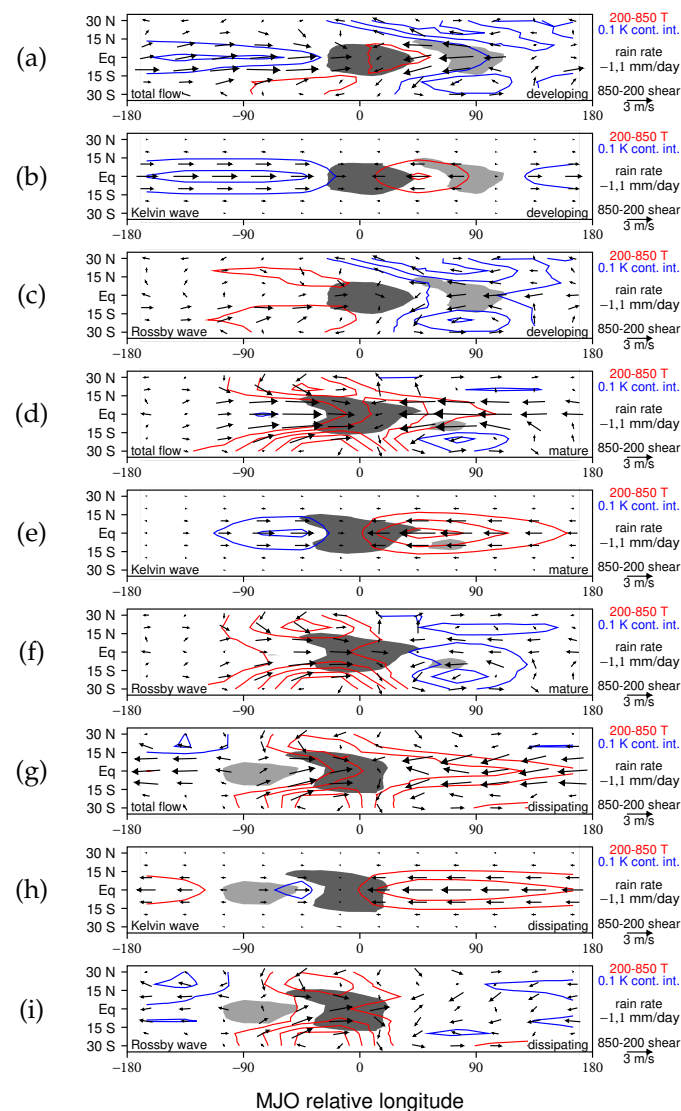


**Figure 3.** The composite MJO and its Kelvin and Rossby wave components for the developing (a–c), mature (d–f), and dissipating (g–i) stages respectively. Mean 200–850 hPa temperature is contoured, vectors indicate the difference between 850 and 200 hPa flow, and rainfall greater than 1 mm/day (less than  $-1$  mm/day) is shaded dark (light) gray.

By the mature stage, the negative phase responses to the suppressed region to the east of the MJO have weakened and shrunk in areal coverage, and their forcing is mostly gone (Figure 3d–f). In contrast, both the positive phase Kelvin wave and Rossby gyres emanating from the convective envelope have grown in scale and amplitude (Figure 3e,f). The Kelvin wave continues to grow in zonal extent in the dissipating stage (Figure 3g,h), as the positive equatorial temperature anomaly and easterly low-level flow have spread more than halfway around the world by this time. In contrast, from the mature to dissipating stage, there is little change in the structure of the Rossby gyres, which appear to be moving along with the convective envelope (i.e., eastward at 5 m/s). As noted by [31], this is probably because the gyres extend poleward into regions with strong westerly winds, and it actually may be the convective envelope that follows the Rossby gyres owing to meridional moisture advection and surface fluxes enhancement in the equatorial westerlies [50–53].

While the structure of temperature and wind perturbations at the mature stage resembles those in the MG model (Figure 3d), this circulation is not in a steady state, and this statement can only be made for this snapshot of the MJO structure. Throughout the convective life cycle, Kelvin wave fronts of both signs propagate around the world (Figure 3b,e,h),

as free tropospheric dissipation is apparently much lower than that typically assumed in the MG model of MJO circulations. A more accurate simple model of MJO circulations comes from interpreting them in terms of the simulation presented in Figure 2. The suppressed region ahead of the convective envelope (Figure 1) generates a negative phase Kelvin wave that propagates around the world (Figure 3b) and Rossby gyres in its vicinity (Figure 3c). Later, positive phase Kelvin waves and Rossby gyres grow from the convective envelope, with the former propagating most of the way around the world by the dissipating stage (Figure 3e–i).

### 3.2. Kelvin and Rossby Wave Impacts on TC Genesis

Now that we have examined a dynamical decomposition of MJO circulations over the life cycle of the convective envelope, we are in a position to interpret changes to TC genesis in terms of the two fundamental components of the MJO's circulation: Kelvin and Rossby waves. In Figure 4, we plot points of TC genesis during 1979–2014 as green dots in the frame of reference of the MJO convective envelope for each of the developing, mature, and dissipating stages. In this figure, regions of perturbation rainfall greater than 1 (2) mm/day are shaded light (dark) gray for the composite MJO. A quick glance at the three figure panels reveals a cluster of TC genesis points on the poleward edges of the MJO precipitation envelope that extends westward for each stage (Figure 4a–c). The tendency of TCs to form in this location has been noted in many previous studies (e.g., [17,29,30]), and it is intuitive in the sense that a minimum ambient rotation is necessary for TC formation, as is moist convection and some sort of pre-cursor disturbance. Moreover, incipient TCs often move westward, while the MJO continues eastward, which explains why the dots extend westward from the edges of the precipitation envelope.

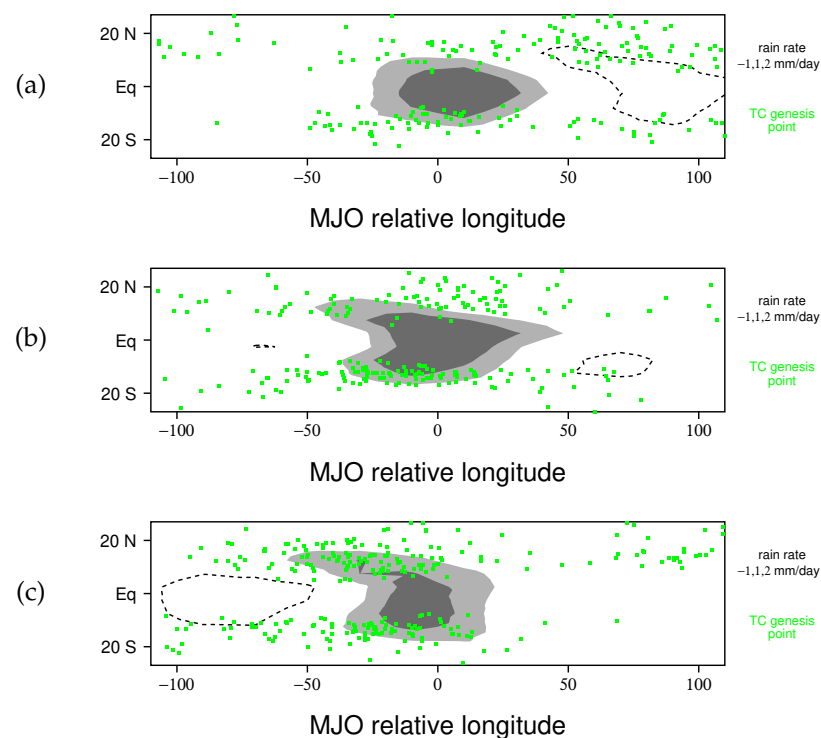


**Figure 4.** Locations of TC genesis (green dots) in the frame of reference of the MJO convective envelope for the developing (a), mature (b), and dissipating (c) stages, respectively. Regions with rainfall greater than 1 (2) mm/day are shaded light (dark) gray, and the  $-1$  mm/day contour is shown with a dashed line.

In the southern hemisphere, there are generally many fewer points of TC genesis away from the MJO convective envelope than there are near it, but in the northern hemisphere,

this is not always the case (Figure 4). Looking at TC genesis patterns for tropical storm seasons for each hemisphere helps to explain this result (Figure 5). In the southern hemisphere, there is a fairly uniform distribution of TC formation from the east coast of Africa to the Central Pacific (Figure 5a). Consequently, the patterning of the MJO overwhelms the smaller variations of the basic state. In contrast, in the northern hemisphere, many more TCs form in the western and Eastern Pacific than in the Central Pacific (Figure 5b), and these signals show up in the MJO frame of the reference in different places in the different stages (i.e., because the MJO convective envelope is typically centered in the Indian Ocean during the developing stage and usually in the western or Central Pacific during the dissipating stage). Therefore, in order to isolate the MJO's impact on TC genesis frequency, we divide the observed number of genesis points by the expected number based on the monthly climatology and group the results by longitude (Figure 6). Interestingly, the general shape of patterning is the same for each stage of the convective life cycle; in each case, there is a region roughly 90 degrees wide with enhanced TC genesis near and to the west of the convective center, and an even broader region with reduced TC genesis to the east of the convective center (Figure 6). The blue line in Figure 6 shows the average over all three stages, and individual stages are not drastically different from the average in the vicinity of the convective envelope. Note that both the enhancement of TC genesis to the west of the MJO, and the reduction to its east, are significant at the 95% confidence level (blue boxes denote significant values).

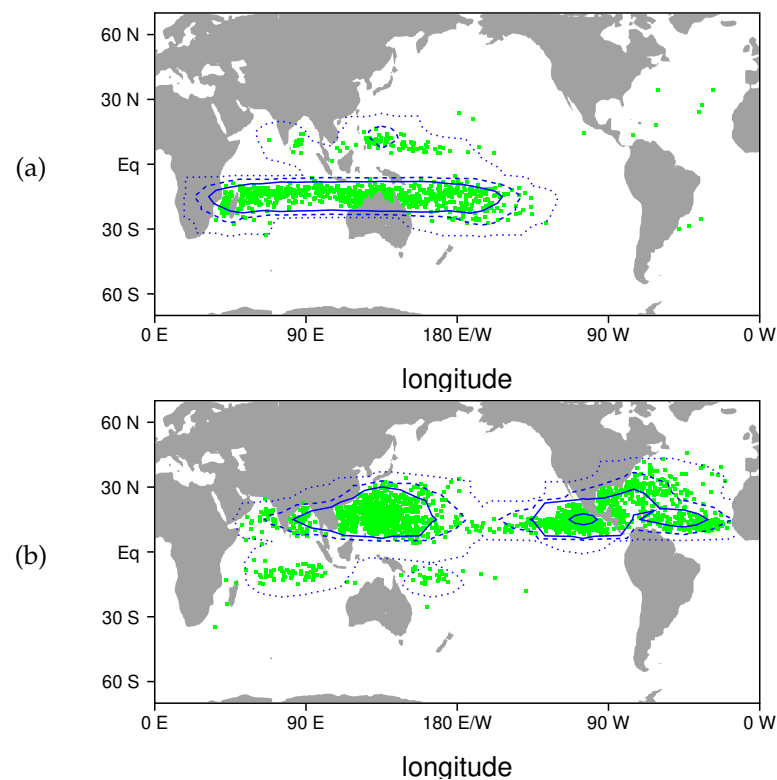


**Figure 5.** Locations of TC genesis (green dots) for the southern (a) and northern hemisphere (b) tropical storm seasons (December through March and May through November, respectively) for 1979–2014. (a) Contours are shown for 4, 20, and 40 storms per latitude/longitude bin. (b) Contours are shown for 7, 35, and 70 storms per latitude/longitude bin. Bins span 30 degrees in longitude and 10 degrees in latitude.

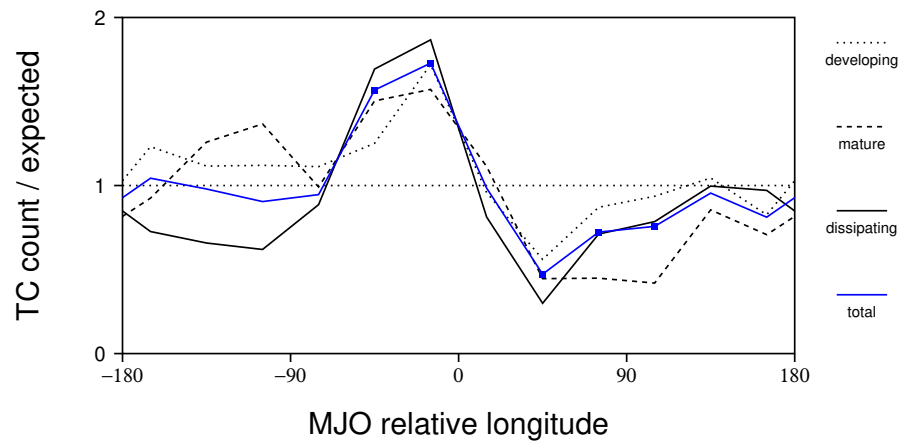


**Figure 6.** The number of TC genesis points divided by the expected number based on monthly climatology for the developing (dotted), mature (dashed), and dissipating (black) stages of the MJO. The blue line shows the average over all of the stages, with points significant at the 95% confidence level marked with blue boxes. TC genesis counts and climatologies are counted over 30-degree wide longitude bins (including all latitudes).

Since the patterning of TC genesis is not that different from one stage of the life cycle of the convective envelope to the next (Figure 6), and using more data reduces noise, to examine the spatial structure of TC genesis modulation, we group all three stages together (Figure 7). The general pattern that emerges is TC genesis is around twice as likely as the climatological value near the equator in a large region centered 30 degrees west of the convective envelope, and less than half as likely as normal near the equator from 40 to 120 degrees east of the convective envelope. In other words, TC genesis is more than four times more likely just west of the MJO convective envelope than it is one-third the circumference of the world to the east of this region (Figure 7). This figure also provides an explanation for the “wings” in the precipitation pattern that extend westward from the main precipitation envelope at latitudes near 15 S and 15 N. There is a high density of TC formation in these areas (Figure 7), and many of these storms have a westward component to their motion and cause rainfall after the MJO’s equatorial precipitation envelope has moved east.

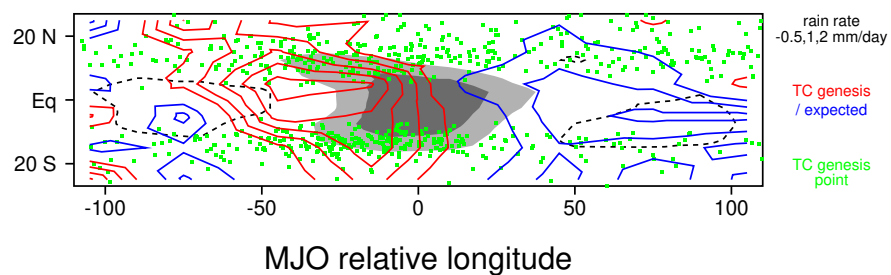


**Figure 7.** The number of TC genesis points divided by the expected number based on monthly climatology for all stages of the MJO. TC genesis counts and climatologies are counted over bins 30 degrees wide in longitude and 10 degrees wide in latitude. Red contours are shown for ratios of 1.3, 1.6, 1.9, 2.2, 2.5, and blue contours are shown for ratios of 0.1, 0.4, 0.7.

We now return to the question of what causes the patterning of TC genesis during each stage of the life cycle of the convective envelope using our Kelvin/Rossby decomposition of MJO circulations. Figure 8 shows Kelvin wave circulations for the developing, mature, and dissipating stages, along with points of TC genesis. For each stage, the Kelvin wave generates low-level convergence (upper-level divergence) of zonal wind centered roughly 15 degrees west of the middle of the convective envelope. By continuity, this circulation is consistent with a deep tropospheric upward motion. Haertel [50] used atmospheric

budgets to show that vertical moisture advection associated with this component of the MJO's circulation generates most of the rainfall in the MJO. Note that this circulation is not entirely a response to the MJO's convection; rather, the cool phase Kelvin wave impinging from the west is a response to the suppressed region ahead of the MJO that has circumnavigated the world (Figures 1 and 3; [31]). While the Kelvin wave convergence and upward motion are the strongest near the equator, as is the relative patterning of TC genesis (Figure 7), the circulation is still fairly strong, 10–15 degrees off the equator where TC genesis peaks. For example, Haertel [50] showed that the Kelvin wave circulation alone contributed a 1–2 mm/day perturbation in rainfall in this region. For each stage of the MJO, there is a cluster of TC genesis points where there is low-level zonal wind convergence (Figure 8). In particular, in the southern hemisphere, where basic state TC genesis is fairly uniform over the MJO's convectively active region (Figure 5a), it is quite apparent that there is a much higher concentration of TC genesis points where the Kelvin wave contributes upward motion than elsewhere.

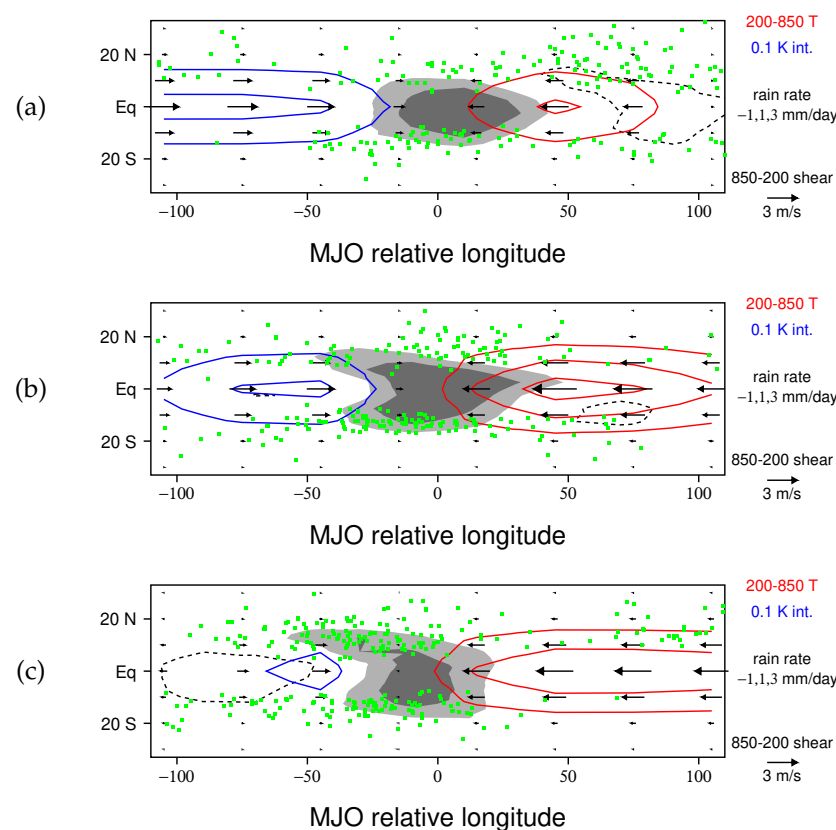


**Figure 8.** TC genesis locations (green dots) and Kelvin wave structure for the developing (a), mature (b), and dissipating (c) stages of the MJO. Contours and vectors are as in Figure 3, and shading is as in Figure 4.

In addition to causing upward motion centered just west of the center of the heaviest rainfall, the Kelvin wave circulation also causes a region of subsidence associated with a Kelvin wave front that advances eastward from the convective envelope and leaves a warmer and drier free troposphere in its wake. In the developing stage (Figure 8a), there is a large negative rainfall perturbation near the Kelvin wave front, and in the mature stage, there is a smaller negative rainfall perturbation near the warmest part of the Kelvin wave (Figure 8b). It is likely that the subsidence, warmth, and dryness associated with the propagating Kelvin wave front are responsible for the reduced TC genesis to the east of the MJO's convective envelope (Figures 6–8).

Figure 9 shows the Rossby wave circulation for the developing, mature, and dissipating stages of the convective envelope along with points of TC genesis for 1979–2014.

A preferred location of TC formation for each stage is from the poleward edges of the equatorial westerlies associated with the Rossby gyres located to the west of the convective envelope, extending eastward into the confluence region between positive and negative phase Rossby gyres. Several previous studies have noted that TCs tend to form where the MJO's Rossby gyres generate low-level vorticity (e.g., [21,30]). Even though each stage has the same duration by definition (Figure 1), there are more TC formations in the mature and dissipating stages when the Rossby gyres are stronger, especially in the southern hemisphere (compare densities of green dots to the west of the MJO in Figure 9a–c). Just as TC genesis is enhanced near the positive phase Rossby gyres to the west of the MJO, it is also reduced near the negative phase Rossby gyres to the east of the MJO (Figures 6, 7, and 9a–c).

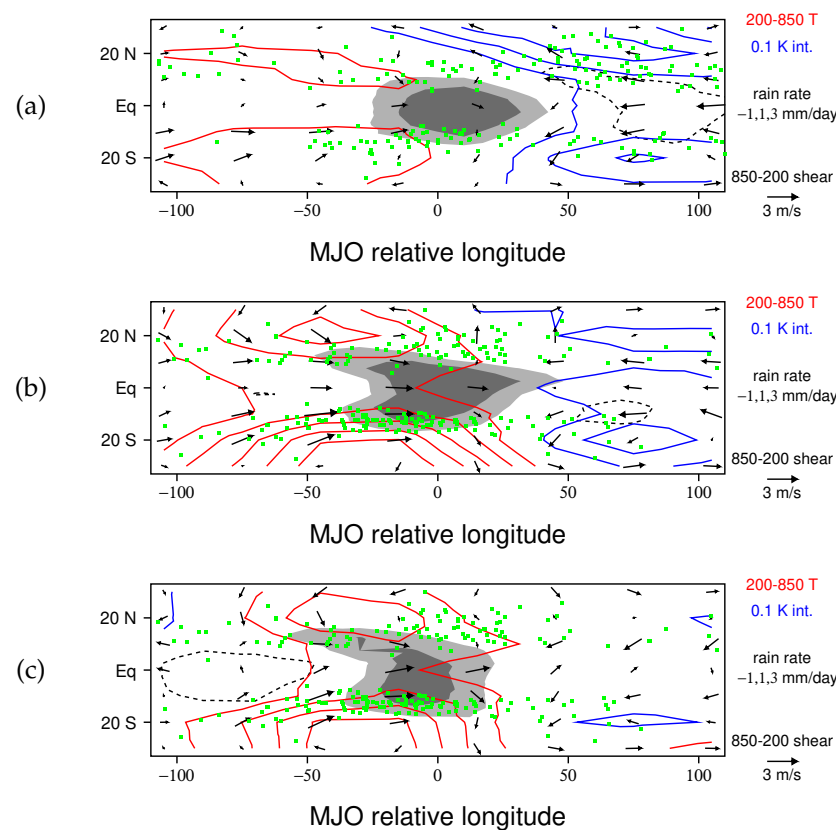
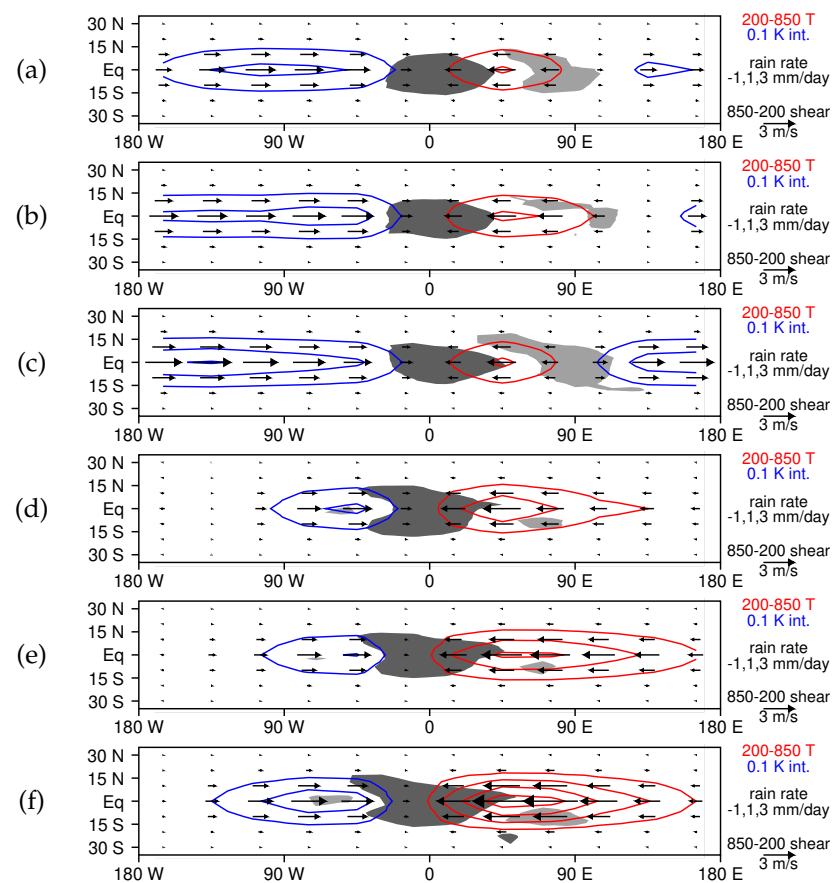


**Figure 9.** TC genesis locations (green dots) and Rossby wave structure for the developing (a), mature (b), and dissipating (c) stages of the MJO. Contours and vectors are as in Figure 3, and shading is as in Figure 4.

### 3.3. Changes in MJO Circulations and TC Impacts over Time

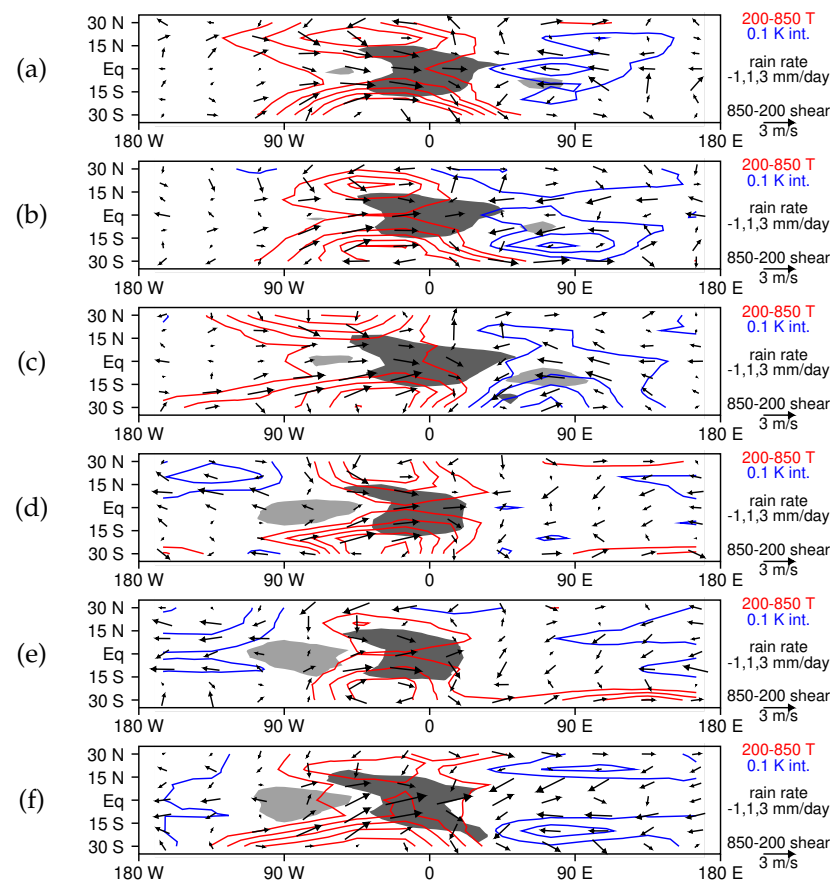
The author's recent modeling/theoretical work suggested that the MJO Kelvin wave circulation may increase with time. In particular, heat and moisture budgets reveal that surface fluxes contribute energy to both positive and negative phases circumnavigating Kelvin waves generated by the MJO [50]. Owing to the nonlinear nature of the Clapeyron–Clausius equation, surface fluxes of moisture are expected to increase substantially as the oceans warm, which could strengthen the MJO [54]. In the Lagrangian-coupled model, simulations with increasing greenhouse gases, MJO circulations intensify with time, with the circumnavigating Kelvin wave amplifying the most [43]. However, not all climate models predict that MJO circulations will intensify with time [55]. Since the data used in this study span 36 years, and 10–12 years worth of data are sufficient for obtaining stable MJO composites [54], we elected to divide our data into three 12-year periods, and construct MJO composites for each period, to determine if the MJO Kelvin wave circulation is increasing with time.

Figure 10a–c show the circumnavigating cool-phase Kelvin wave for the developing phase of the MJO for the periods 1979–1990, 1991–2002, and 2003–2014, respectively. This wave, which lies to the west of the developing MJO convective envelope, grew in zonal extent and amplitude during the 36-year period. Figure 10d–f show the warm phase Kelvin wave that grew eastward from the MJO convective envelope during the mature phases for the same three time periods. This wave also appeared to intensify during the 36-year period. While random variations could cause these changes (i.e., a longer period of growth would be necessary to establish a trend), the theoretical, modeling, and observational results provide substantial evidence that the circumnavigating Kelvin wave component of the MJO becomes stronger as the oceans warm (Figure 10; [43,50,54,56]).



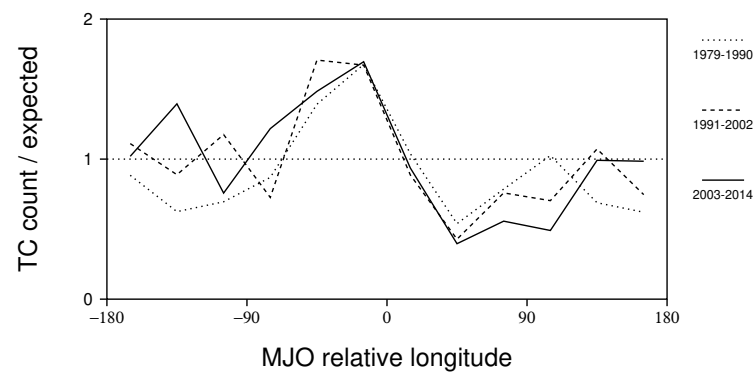
**Figure 10.** The change in the MJO Kelvin wave circulation over 1979–2014. Kelvin wave structure during the developing stage for 1979–1990 (a), 1991–2002 (b), and 2003–2014 (c). The Kelvin wave structure during the mature stage for 1979–1990 (d), 1991–2002 (e), and 2003–2014 (f). Contours, vectors, and shading are as in Figure 3.

Figure 11 shows the structure of the Rossby gyres for the mature and dissipating phases of the MJO for the same three time periods. While the Rossby gyres in the last 12-year period are the largest and the strongest for both the mature and dissipating stages (Figure 11c,f), they are also fairly strong in the first 12-year period (Figure 11a,d), so there is no clear trend in changes with respect to time. Moreover, our previous theoretical and modeling results do not make any clear predictions about how the Rossby gyres will change with time.



**Figure 11.** The change in the MJO Rossby wave circulation over 1979–2014. Rossby wave structure during the mature stage for 1979–1990 (a), 1991–2002 (b), and 2003–2014 (c). Rossby wave structure during the dissipating stage for 1979–1990 (d), 1991–2002 (e), and 2003–2014 (f). Contours, vectors, and shading are as in Figure 3.

Since the MJO's Kelvin wave circulation appears to have intensified during the 36-year period considered here, we now examine the patterning of TC genesis during this time for similar trends (Figure 12). To the east of the MJO, the reduction in TC genesis increases in amplitude during the 36-year period. This is what one would expect from the amplification of the warm phase Kelvin wave extending eastward from the convective envelope (Figure 10d–f). While the enhancement of TC genesis to the west of the convective envelope is generally greater in 2003–2014 than it is in 1979–1990 (compare solid and dotted lines in Figure 12), around 45 degrees west of the convective center the enhancement of TC genesis is actually the greatest in 1991–2002. However, the signal in this region is quite noisy, which makes it difficult to discern a trend. We conclude that while the reduction of TC genesis to the east of the MJO has amplified along with the warm phase Kelvin wave in that location, there is not a clear trend in the enhancement of TC genesis to the west of the convective envelope in the period of time considered here.



**Figure 12.** The change in MJO patterning of TC genesis over 1979–2014. TC genesis counts divided by expected values based on monthly climatology for 1979–1990 (dotted), 1991–2002 (dashed), and 2003–2014 (solid). TC genesis counts and climatologies are counted over 30-degree wide longitude bins (including all latitudes). All stages are grouped together.

#### 4. Discussion

In this study, we examine the relationship between MJO impacts on TC genesis, and the two fundamental components of the MJO's planetary-scale circulation: the Kelvin and the Rossby wave. These circulations spin up in response to the MJO's convective heating, and accordingly, we study their impact on TC formation in the frame of reference of the MJO convective envelope using stages based on its life cycle.

In the first part of this study, we create a new composite of MJO circulations using atmospheric-sounding stations for a 36-year period in which satellite observations of rainfall are available. The MJO convective envelope is identified by tracking large-scale eastward moving rainfall perturbations using data filtered for MJO time scales. Circulations are composited for each of the three phases of the convective envelope: the developing, mature, and dissipating stages. This analysis reveals a negative phase Kelvin/Rossby couplet associated with the suppressed region ahead of the MJO (Figure 3a–c), which is followed by a positive phase Kelvin/Rossby couplet that grows from the convective envelope (Figure 3d–i). Unlike the circulations in the classical Matsuno–Gill model of the MJO (Matsuno 1966; Gill 1980), the Kelvin waves expand eastward as long as the forcing is in place (i.e., Kelvin wave fronts propagate around the world), and after the forcing decays, the Kelvin and Rossby waves separate.

In the second part of this study, we analyze perturbations to TC genesis in the frame of reference of the convective envelope, and relate them to Kelvin and Rossby wave circulations. TC genesis is enhanced in a region on the poleward edges of the convective envelope that extends westward for each phase of the life cycle. In all three stages, the Kelvin wave circulation contributes upward motion in this region, which lies at the intersection of a cool phase Kelvin wave impinging from the west and warm phase Kelvin wave growing to the east (Figure 8). In later stages, the Rossby wave contributes low-level vorticity as TC enhancement occurs near the poleward edges of the low-level westerlies associated with the Rossby gyres (Figure 9).

Both Kelvin and Rossby waves also contribute to the reduction of TC genesis to the east of the MJO convective envelope. As the Kelvin wave front propagates eastward from the growing convective envelope, it produces subsidence, which is accompanied by reduced rainfall, and leaves a warmer and drier free troposphere in its wake (Figure 8). During the developing and mature stages of the convective envelope, there are also cool-phase anticyclonic Rossby gyres with equatorial easterlies, which were generated by the suppressed region ahead of the convective envelope (Figures 1 and 9), and which also inhibit TC genesis.

We also examined how the Kelvin and Rossby wave circulations changed during the 36-year period for which data were available. During this time, the MJO's Kelvin wave circulation increased in amplitude (Figure 10), as predicted by modeling and theory in

several previous studies [31,50,54]. The reduction in TC genesis to the east of the MJO also became more pronounced during this time (Figure 12). There was no clear trend in changes to the Rossby wave circulation (Figure 11) or the enhancement of TC genesis to the west of the MJO's convective envelope (Figure 12), however.

While the most obvious application of the research presented here relates to the modulation TCs in the Indo-Pacific region, where the MJO is convectively active, these results also help to explain the more remote modulation of TCs in the Eastern Pacific and Atlantic regions. Of the two circulation components of the MJO, the Kelvin wave circulation is much stronger in remote regions than the Rossby wave (Figure 3). During the mature stage, the warm phase Kelvin wave generates a broad region of subsidence on its leading edge that leaves in its wake a warmer and drier troposphere (Figure 3e). TC genesis points are sparse in this region (Figure 8b), with the greatest relative reduction of TC genesis occurring 105 degrees east of the convective envelope (Figure 6, dashed line). For a typical Western Pacific location of the MJO convective envelope during the mature phase, this equates to a substantial reduction of TC genesis in the Eastern Pacific. Maloney and Hartmann [26] previously noted that a minimum in hurricane activity occurs in the Eastern Pacific when MJO convection is active in the West Pacific, and attributed this modulation to zonal wind variations associated with Kelvin wave propagation. Klotzbach and Oliver [28] also noted that accumulated cyclone energy in the Atlantic is at a minimum during MJO phases 5–7, which is when the convective envelope moves from the Maritime continent into the Western Pacific. Since the dynamics of the MJO's Kelvin wave circulation are linear [31], it is likely that the same mechanism causes an increase in TCs in the Eastern Pacific and Atlantic when convection is suppressed by the MJO over the Western Pacific [26,27].

This paper provides a dynamical framework for understanding MJO impacts on TC genesis, intensification, and landfall reported in previous studies. It builds on the work of Maloney and Hartmann [26] and Barrett and Leslie [27]; they previously showed that the MJO's Kelvin wave circulation modulates TC genesis in the Eastern Pacific and Atlantic, and also reveals enhancement and reduction of TC genesis where the Kelvin contributes upward and downward motion, respectively, in the immediate vicinity of the convective envelope, which typically moves from the Indian Ocean to the West Pacific. Note that this conclusion is not contradictory to those of previous studies that attributed enhanced TC genesis to high humidity [29], upward motion [30], and more precursor disturbances [17], as the ascending branch of the Kelvin wave circulation first moistens by vertical advection, and then enhances rainfall, which means more convective systems of all types [50]. The results presented here also validate previous studies that related TC enhancement to low-level vorticity associated with the Rossby gyres just west of the convective envelope [20–22,30], as the greatest enhancement of TC genesis occurs in the mature and dissipating stages of the convective envelope where upward motion associated with the Kelvin wave is superposed with low-level vorticity enhancement from the Rossby gyres (Figures 6–9). One point that is emphasized in this paper, which is not always discussed in previous studies, is how Kelvin and Rossby waves also act to reduce TC genesis ahead of the convective envelope.

Because the Kelvin and Rossby wave components of the MJO's circulation are ultimately responsible for many of the intraseasonal changes to TC formation and intensification, and these circulation features evolve slowly over time and are somewhat predictable, it would make sense to diagnose these wave components as part of the process of making short to medium-range TC forecasts. While such forecasts already make use of the current phase of the MJO (e.g., from an RMM index), the formation and dissipation locations of individual MJO convective envelopes differ from one MJO to the next, as do the positioning, zonal extent, and phases of Kelvin and Rossby wave circulations. Precise information on these circulation components could help forecasters more precisely predict where TC formation and intensification will be enhanced or inhibited.

**Funding:** This research was funded by the National Science Foundation grant AGS-2140281.

**Data Availability Statement:** The tropical cyclone data used for this study is available at <https://www.ncei.noaa.gov/products/international-best-track-archive> (accessed on 20 June 2023).

**Acknowledgments:** The IGRA version 2 atmospheric-sounding data used in this study were provided by Maria Gehne of the NOAA Physical sciences laboratory.

**Conflicts of Interest:** The author declares no conflict of interest.

## References

1. Madden, R.A.; Julian, P.R. Detection of a 40–50 day oscillation in the zonal wind in the tropical Pacific. *J. Atmos. Sci.* **1971**, *28*, 702–708. [[CrossRef](#)]
2. Madden, R.A.; Julian, P.R. Description of global-scale circulation cells in the tropics with a 40–50 day period. *J. Atmos. Sci.* **1972**, *29*, 1109–1123. [[CrossRef](#)]
3. Madden, R.A.; Julian, P.R. Observations of the 40–50-day tropical oscillation—A review. *Mon. Weather Rev.* **1994**, *122*, 814–837. [[CrossRef](#)]
4. Zhang, C. Madden-Julian oscillation. *Rev. Geophys.* **2005**, *43*, RG2003. [[CrossRef](#)]
5. Wheeler, M.; Kiladis, G.N.; Webster, P.J. Large-scale dynamical fields associated with convectively coupled equatorial waves. *J. Atmos. Sci.* **2000**, *57*, 613–640. [[CrossRef](#)]
6. Sobel, A.; Kim, D. The MJO-Kelvin wave transition. *Geophys. Res. Lett.* **2012**, *39*, L20808. [[CrossRef](#)]
7. Haertel, P.; Straub, K.; Budsock, A. Transforming circumnavigating Kelvin waves that initiate and dissipate the Madden-Julian Oscillation. *Q. J. R. Meteorol. Soc.* **2015**, *141*, 1586–1602. [[CrossRef](#)]
8. Wu, M.L.C.; Schubert, S.; Huang, N.E. The development of the South Asian summer monsoon and the intraseasonal oscillation. *J. Clim.* **1999**, *12*, 2054–2075. [[CrossRef](#)]
9. Lorenz, D.J.; Hartmann, D.L. The effect of the MJO on the North American monsoon. *J. Clim.* **2006**, *19*, 333–343. [[CrossRef](#)]
10. Haertel, P.; Boos, W.R. Global association of the Madden-Julian Oscillation with monsoon lows and depressions. *Geophys. Res. Lett.* **2017**, *44*, 8065–8074. [[CrossRef](#)]
11. Mundhenk, B.D.; Barnes, E.A.; Maloney, E.D.; Baggett, C.F. Skillful empirical subseasonal prediction of landfalling atmospheric river activity using the Madden-Julian oscillation and quasi-biennial oscillation. *NPJ Clim. Atmos. Sci.* **2018**, *1*, 1–7. [[CrossRef](#)]
12. Liang, Y.; Fedorov, A.V. Linking the Madden-Julian Oscillation, tropical cyclones and westerly wind bursts as part of El Niño development. *Clim. Dyn.* **2021**, *57*, 1039–1060. [[CrossRef](#)]
13. Liang, Y.; Fedorov, A.V.; Haertel, P. Intensification of Westerly Wind Bursts Caused by the Coupling of the Madden-Julian Oscillation to SST During El Niño Onset and Development. *Geophys. Res. Lett.* **2021**, *48*, e2020GL089395. [[CrossRef](#)]
14. Hu, S.; Fedorov, A.V. The extreme El Niño of 2015–2016: The role of westerly and easterly wind bursts, and preconditioning by the failed 2014 event. *Clim. Dyn.* **2019**, *52*, 7339–7357. [[CrossRef](#)]
15. Waliser, D.; Lau, K.; Stern, W.; Jones, C. Potential predictability of the Madden-Julian oscillation. *Bull. Am. Meteorol. Soc.* **2003**, *84*, 33–50. [[CrossRef](#)]
16. Neena, J.; Lee, J.Y.; Waliser, D.; Wang, B.; Jiang, X. Predictability of the Madden-Julian oscillation in the intraseasonal variability hindcast experiment (ISVHE). *J. Clim.* **2014**, *27*, 4531–4543. [[CrossRef](#)]
17. Liebmann, B.; Hendon, H.H.; Glick, J.D. The relationship between tropical cyclones of the Western Pacific and Indian Oceans and the Madden-Julian oscillation. *J. Meteorol. Soc. Jpn. Ser. II* **1994**, *72*, 401–412. [[CrossRef](#)]
18. Kim, J.H.; Ho, C.H.; Kim, H.S.; Sui, C.H.; Park, S.K. Systematic variation of summertime tropical cyclone activity in the western North Pacific in relation to the Madden-Julian oscillation. *J. Clim.* **2008**, *21*, 1171–1191. [[CrossRef](#)]
19. Chen, J.M.; Wu, C.H.; Chung, P.H.; Sui, C.H. Influence of intraseasonal–interannual oscillations on tropical cyclone genesis in the western North Pacific. *J. Clim.* **2018**, *31*, 4949–4961. [[CrossRef](#)]
20. Hall, J.D.; Matthews, A.J.; Karoly, D.J. The modulation of tropical cyclone activity in the Australian region by the Madden-Julian oscillation. *Mon. Weather Rev.* **2001**, *129*, 2970–2982. [[CrossRef](#)]
21. Bessafi, M.; Wheeler, M.C. Modulation of south Indian Ocean tropical cyclones by the Madden-Julian oscillation and convectively coupled equatorial waves. *Mon. Weather Rev.* **2006**, *134*, 638–656. [[CrossRef](#)]
22. Krishnamohan, K.; Mohanakumar, K.; Joseph, P. The influence of Madden-Julian oscillation in the genesis of north Indian Ocean tropical cyclones. *Theor. Appl. Climatol.* **2012**, *109*, 271–282. [[CrossRef](#)]
23. Wheeler, M.C.; Hendon, H.H. An all-season real-time multivariate MJO index: Development of an index for monitoring and prediction. *Mon. Weather Rev.* **2004**, *132*, 1917–1932. [[CrossRef](#)]
24. Girishkumar, M.; Suprit, K.; Vishnu, S.; Prakash, V.T.; Ravichandran, M. The role of ENSO and MJO on rapid intensification of tropical cyclones in the Bay of Bengal during October–December. *Theor. Appl. Climatol.* **2015**, *120*, 797–810. [[CrossRef](#)]
25. Bhardwaj, P.; Singh, O.; Pattanaik, D.; Klotzbach, P.J. Modulation of Bay of Bengal tropical cyclone activity by the Madden-Julian oscillation. *Atmos. Res.* **2019**, *229*, 23–38. [[CrossRef](#)]
26. Maloney, E.D.; Hartmann, D.L. Modulation of eastern North Pacific hurricanes by the Madden-Julian oscillation. *J. Clim.* **2000**, *13*, 1451–1460. [[CrossRef](#)]
27. Barrett, B.S.; Leslie, L.M. Links between tropical cyclone activity and Madden-Julian oscillation phase in the North Atlantic and northeast Pacific basins. *Mon. Weather Rev.* **2009**, *137*, 727–744. [[CrossRef](#)]

28. Klotzbach, P.J.; Oliver, E.C. Modulation of Atlantic basin tropical cyclone activity by the Madden–Julian oscillation (MJO) from 1905 to 2011. *J. Clim.* **2015**, *28*, 204–217. [[CrossRef](#)]
29. Camargo, S.J.; Wheeler, M.C.; Sobel, A.H. Diagnosis of the MJO modulation of tropical cyclogenesis using an empirical index. *J. Atmos. Sci.* **2009**, *66*, 3061–3074. [[CrossRef](#)]
30. Wang, B.; Moon, J.Y. An anomalous genesis potential index for MJO modulation of tropical cyclones. *J. Clim.* **2017**, *30*, 4021–4035. [[CrossRef](#)]
31. Haertel, P. Kelvin/Rossby wave partition of Madden-Julian oscillation circulations. *Climate* **2020**, *9*, 2. [[CrossRef](#)]
32. Nakazawa, T. Tropical super clusters within intraseasonal variations over the Western Pacific. *J. Meteorol. Soc. Jpn. Ser. II* **1988**, *66*, 823–839. [[CrossRef](#)]
33. Haertel, P.T.; Kiladis, G.N. Dynamics of 2-day equatorial waves. *J. Atmos. Sci.* **2004**, *61*, 2707–2721. [[CrossRef](#)]
34. Kiladis, G.N.; Wheeler, M.C.; Haertel, P.T.; Straub, K.H.; Roundy, P.E. Convectively coupled equatorial waves. *Rev. Geophys.* **2009**, *47*, RG2003. [[CrossRef](#)]
35. Xie, P.; Janowiak, J.E.; Arkin, P.A.; Adler, R.; Gruber, A.; Ferraro, R.; Huffman, G.J.; Curtis, S. GPCP pentad precipitation analyses: An experimental dataset based on gauge observations and satellite estimates. *J. Clim.* **2003**, *16*, 2197–2214. [[CrossRef](#)]
36. Adler, R.F.; Sapiiano, M.R.; Huffman, G.J.; Wang, J.J.; Gu, G.; Bolvin, D.; Chiu, L.; Schneider, U.; Becker, A.; Nelkin, E.; et al. The Global Precipitation Climatology Project (GPCP) monthly analysis (new version 2.3) and a review of 2017 global precipitation. *Atmosphere* **2018**, *9*, 138. [[CrossRef](#)] [[PubMed](#)]
37. Durre, I.; Vose, R.S.; Wuertz, D.B. Overview of the integrated global radiosonde archive. *J. Clim.* **2006**, *19*, 53–68. [[CrossRef](#)]
38. Durre, I.; Yin, X.; Vose, R.S.; Applequist, S.; Arnfield, J. Enhancing the data coverage in the integrated global radiosonde archive. *J. Atmos. Ocean. Technol.* **2018**, *35*, 1753–1770. [[CrossRef](#)]
39. Hung, M.P.; Lin, J.L.; Wang, W.; Kim, D.; Shinoda, T.; Weaver, S.J. MJO and convectively coupled equatorial waves simulated by CMIP5 climate models. *J. Clim.* **2013**, *26*, 6185–6214. [[CrossRef](#)]
40. Jiang, X.; Waliser, D.E.; Xavier, P.K.; Petch, J.; Klingaman, N.P.; Woolnough, S.J.; Guan, B.; Bellon, G.; Crueger, T.; DeMott, C.; et al. Vertical structure and physical processes of the Madden-Julian oscillation: Exploring key model physics in climate simulations. *J. Geophys. Res. Atmos.* **2015**, *120*, 4718–4748. [[CrossRef](#)]
41. Knapp, K.R.; Diamond, H.J.; Kossin, J.P.; Kruk, M.C.; Schreck, C.J. *NCDC International Best Track Archive for Climate Stewardship (IBTrACS) Project, Version 4*; NOAA National Centers for Environmental Information: Hancock County, MI, USA, 2019. [[CrossRef](#)]
42. Knapp, K.R.; Kruk, M.C.; Levinson, D.H.; Diamond, H.J.; Neumann, C.J. The international best track archive for climate stewardship (IBTrACS) unifying tropical cyclone data. *Bull. Am. Meteorol. Soc.* **2010**, *91*, 363–376. [[CrossRef](#)]
43. Haertel, P. Prospects for Erratic and Intensifying Madden-Julian Oscillations. *Climate* **2020**, *8*, 24. [[CrossRef](#)]
44. Emanuel, K.A.; David Neelin, J.; Bretherton, C.S. On large-scale circulations in convecting atmospheres. *Q. J. R. Meteorol. Soc.* **1994**, *120*, 1111–1143. [[CrossRef](#)]
45. Wheeler, M.; Kiladis, G.N. Convectively coupled equatorial waves: Analysis of clouds and temperature in the wavenumber–frequency domain. *J. Atmos. Sci.* **1999**, *56*, 374–399. [[CrossRef](#)]
46. Haertel, P.T.; Kiladis, G.N.; Denno, A.; Rickenbach, T.M. Vertical-mode decompositions of 2-day waves and the Madden–Julian oscillation. *J. Atmos. Sci.* **2008**, *72*, 813–833. [[CrossRef](#)]
47. Fulton, S.R.; Schubert, W.H. Vertical normal mode transforms: Theory and application. *Mon. Weather Rev.* **1985**, *113*, 647–658. [[CrossRef](#)]
48. Matsuno, T. Quasi-geostrophic motions in the equatorial area. *J. Meteorol. Soc. Jpn. Ser. II* **1966**, *44*, 25–43. [[CrossRef](#)]
49. Gill, A. Some simple solutions for heat-induced tropical circulation. *Q. J. R. Meteorol. Soc.* **1980**, *106*, 447–462. [[CrossRef](#)]
50. Haertel, P. Kelvin and Rossby Wave Contributions to the Mechanisms of the Madden–Julian Oscillation. *Geosciences* **2022**, *12*, 314. [[CrossRef](#)]
51. Lin, X.; Johnson, R.H. Heating, moistening, and rainfall over the Western Pacific warm pool during TOGA COARE. *J. Atmos. Sci.* **1996**, *53*, 3367–3383. [[CrossRef](#)]
52. Sobel, A.; Maloney, E. Moisture modes and the eastward propagation of the MJO. *J. Atmos. Sci.* **2013**, *70*, 187–192. [[CrossRef](#)]
53. Adames, Á.F.; Wallace, J.M. Three-dimensional structure and evolution of the moisture field in the MJO. *J. Atmos. Sci.* **2015**, *72*, 3733–3754. [[CrossRef](#)]
54. Haertel, P. Sensitivity of the Madden Julian Oscillation to Ocean Warming in a Lagrangian Atmospheric Model. *Climate* **2018**, *6*, 45. [[CrossRef](#)]
55. Maloney, E.D.; Adames, Á.F.; Bui, H.X. Madden–Julian oscillation changes under anthropogenic warming. *Nat. Clim. Chang.* **2019**, *9*, 26–33. [[CrossRef](#)]
56. Fuchs, Ž.; Raymond, D.J. A simple model of intraseasonal oscillations. *J. Adv. Model. Earth Syst.* **2017**, *9*, 1195–1211. [[CrossRef](#)]

**Disclaimer/Publisher’s Note:** The statements, opinions and data contained in all publications are solely those of the individual author(s) and contributor(s) and not of MDPI and/or the editor(s). MDPI and/or the editor(s) disclaim responsibility for any injury to people or property resulting from any ideas, methods, instructions or products referred to in the content.